Editors' Suggestion

Breakup and Recovery of Topological Zero Modes in Finite Non-Hermitian Optical Lattices

Wange Song,[1,3] Wenzhao Sun,[2] Chen Chen,[1,3] Qinghai Song,[2] Shumin Xiao,[2] Shining Zhu,[1,3] and Tao Li[1,3,*]

[1]*National Laboratory of Solid State Microstructures, Key Laboratory of Intelligent Optical Sensing and Integration, Jiangsu Key Laboratory of Artificial Functional Materials, College of Engineering and Applied Sciences, Nanjing University, Nanjing 210093, China*

[2]*State Key Laboratory on Tunable Laser Technology, Ministry of Industry and Information Technology, Key Lab of Micro-Nano Optoelectronic Information System, Shenzhen Graduate School, Harbin Institute of Technology, Shenzhen 518055, China*

[3]*Collaborative Innovation Center of Advanced Microstructures, Nanjing 210093, China*

(Received 2 February 2019; published 14 October 2019)

The topological edge state (TES) in a one-dimensional optical lattice has exhibited robust field localization or waveguiding against the structural perturbations that would give rise to fault-tolerant photonic integrations. However, the zero mode as a kind of TES usually deviates from the exact zero-energy state in a finite Hermitian lattice due to the coupling between these edge states, which inevitably weaken the topological protection. Here, we first show such a breakup of zero modes in finite Su-Schriffer-Heeger optical lattices and then reveal their recovery by introducing non-Hermitian degeneracies with parity-time (PT) symmetry. We carry out experiments in a finite silicon waveguide lattice, where a passive-PT symmetry was implemented with carefully controlled lossy silicon waveguides. The experimental results are fully compatible with the theoretical prediction. Our results show that the topological property of an open system can be tuned by non-Hermitian lattice engineering, which offers a route to enhance the topological protection in a finite system.

DOI: 10.1103/PhysRevLett.123.165701

Parity-time (PT) symmetric systems with non-Hermitian Hamiltonians have received increasing attention over the past decade [1–12]. On crossing the transition point [i.e., the exceptional point (EP) [2,3]], the spectrum is no longer purely real due to spontaneous PT-symmetry breaking. Among various PT-symmetric systems, PT photonics with intentionally modulated gain and loss has become an attractive topic [4,5], which has witnessed a series of novel optical phenomena and functionalities [6–12]. On the other hand, topological photonics has sparked a great deal of interest with intriguing phenomena associated with the topological edge states (TESs) [13–15]. The dimensionless edge state with its eigenenergy pinned at the middle of a gapped band structure is referred to as the zero mode [16], which is expected to work in fault-tolerant waveguiding and quantum computation [17,18]. In fact, topological systems are usually of finite system size, which will weaken the topological protection. For example, zero modes may deviate from the exact-zero energy in a finite Hermitian lattice due to the coupling effect [16], which inevitably leads to weakness of the intriguing topologically protected characteristics. It is necessary to strengthen these zero modes in a finite topological system. Recently, the topological properties of non-Hermitian systems have been studied [19–24] and TESs in non-Hermitian systems are demonstrated [25,26]. Non-Hermitian properties have been proven to give rise to a lot of useful aspects in topological phenomena, such as selective enhancement of topological states [27], non-Hermitian-induced topological protection [28,29], topological insulator lasers [30–33], etc. They provide us with the foundation to investigate a variety of topological phenomena in open systems and a possible route for the recovery of zero modes by non-Hermiticity in finite systems.

In this Letter, we clearly demonstrate both the breakup and recovery of zero modes in a finite 1D topological optical system, where the recovery of zero modes was realized by introducing the loss to form a non-Hermitian topological configuration. We systematically investigated the interplay of PT phases and edge states in the non-Hermitian Su-Schriffer-Heeger (SSH) model [34]. On crossing the EPs, the edge states are driven to undergo a transition from a trivial PT-symmetric edge state to a topological broken-PT one. The experimental results in silicon waveguide lattices with controlled losses are in good agreement with theoretical results. Our study reveals that the topological property of an open system can be tuned by non-Hermitian parameters and implies more interesting physics and photonic applications in PT and topological systems.

We would like to start from a general 1D non-Hermitian SSH model defined by a finite coupled optical waveguide lattice. Figure 1(a) schematically shows the 1D optical lattice with N coupled waveguides, where c_1 and c_2 are two coupling coefficients of the nearest neighbors, and β_G and β_L (where $\beta_G = \beta_0 - i\gamma$, $\beta_L = \beta_0 + i\gamma$, and γ is gain or loss strength) are the on site propagation constants (i.e., on site energy) in the gain and lossy waveguides, respectively. Following the coupled-mode theory (CMT) in the tight-binding approximation, the optical field propagation within the waveguide lattice can be described by

$$\begin{aligned} -i\frac{\partial}{\partial z}\varphi_n &= \beta_L\varphi_n + c_2\varphi_{n-1} + c_1\varphi_{n+1}, \quad n = 1, 3, \ldots, \\ -i\frac{\partial}{\partial z}\varphi_n &= \beta_G\varphi_n + c_1\varphi_{n-1} + c_2\varphi_{n+1}, \quad n = 2, 4, \ldots, \end{aligned} \tag{1}$$

where φ_n denotes the optical field in the nth waveguide. The non-Hermitian bulk Hamiltonian is [29]

$$H(k) = \begin{pmatrix} i\gamma & \rho^*(k) \\ \rho(k) & -i\gamma \end{pmatrix}, \tag{2}$$

where $\rho(k) = c_1 + c_2 \exp(ika)$, k is the quasimomentum in the Brillouin zone, and a is the period.

We first consider the Hermitian cases ($\gamma = 0$), where the SSH Hamiltonian $H(k)$ possesses a chiral symmetry

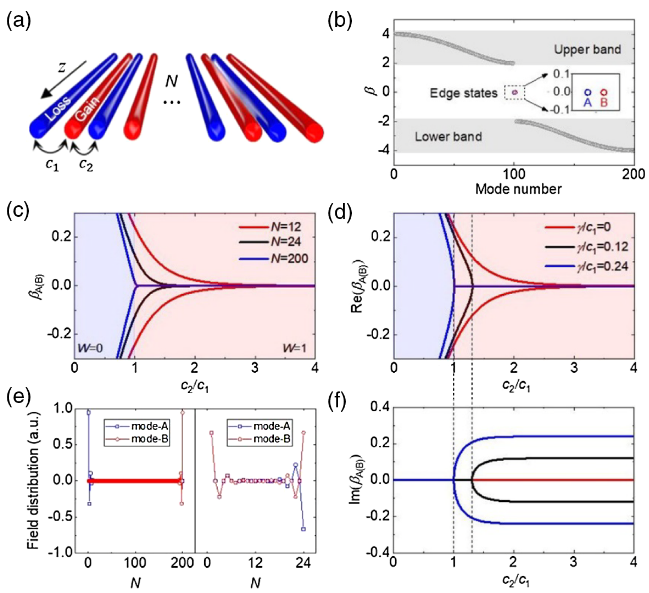

FIG. 1. Breakup and recovery of zero modes by non-Hermitian modulation. (a) Schematics of the 1D finite non-Hermitian SSH model with N waveguides, where red and blue colors indicate the gain and loss, respectively. (b) Band structure with $N = 200$, $c_1 = 1$, $c_2/c_1 = 3$, and $W = 1$. Gray areas indicate the bulk bands. (c) β_A and β_B as a function of c_2/c_1 in the Hermitian cases with different $N(c_1 = 1)$. The red region represents the topologically nontrivial phase and the blue region is the trivial phase. The real (d) and imaginary parts (f) of β_A and β_B as a function of c_2/c_1 in non-Hermitian cases with different γ ($c_1 = 1$, $N = 12$). (e) The eigenmode profiles of exact-zero modes (left) and near-zero modes (right).

$[\sigma_z H(k)\sigma_z = -H(k)$, where σ_i refers to Pauli matrices], and the energy spectrum is symmetric around the zero energy [35]. According to Eqs. (1) and (2), one may obtain the nontrivial TESs in the case of $c_2/c_1 > 1$, which is also indicated by the winding number W [36,37] ($W = 1$ when $c_2 > c_1$ and $W = 0$ when $c_2 < c_1$). Figure 1(b) shows the mode diagram of a lattice of 200 waveguides with $W = 1$ indicating a near infinite system. There are two zero-energy states (blue and red circles) that appear in the midgap between two bands. As the system size decreases (e.g., $N = 24$ and 12), two zero modes will deviate from the exact-zero energy. Figure 1(c) shows the mode constants of two edge states (β_A and β_B) plotted as a function of c_2/c_1. It is clear that, in a case of $c_2/c_1 > 1$, the two edge modes will not preserve exact-zero modes as N decreases. It means that as the optical lattice undergoes from an infinite to finite system, the exact-zero modes will break into nonzero or near-zero modes. We further compare the field distributions of exact- and near-zero modes, with the results shown in Fig. 1(e). Different from single-boundary localization of zero modes, the near-zero modes have a localized field at both boundaries in symmetric or asymmetric manners due to boundary coupling in such a finite system [16,28]. Indeed, these near-zero edge states with two-boundary localization have been demonstrated in the finite zigzag chains of plasmonic and dielectric nanoparticles [38,39].

According to above results and analyses, it is necessary to exploit a route to preserve the exact-zero modes in practical finite systems. Here, we would like to consider the non-Hermitian optical system with gain and loss, where the bulk Hamiltonian $H(k)$ is of PT symmetry $[\sigma_x H(k)^* \sigma_x = H(k)]$ and pseudo-anti-Hermiticity $[\sigma_z H(k)^\dagger \sigma_z = -H(k)]$. The latter symmetry gives rise to pairwise eigenvalues $\beta(k)$ and $-\beta^*(k)$ and can lead to nontrivial topology [22,28], which can be accurately probed by the global Berry phase [19,22,28,29]. In our case, it corresponds to the summation of the complex Berry phase in both lower and upper bands. The Berry phase in each band can be calculated by $\Phi_B^m = \oint_k idk\langle\psi_m(k)|\partial/\partial k|\psi_m(k)\rangle$, which leads to $\Phi_B^m = (\Phi_0/2) \pm \frac{1}{2}\oint_{\phi_k} \cos\gamma_k d\phi_k$ [29]. Here, k is the Bloch wave number within the first Brillouin zone, ψ_m is the eigenstate (m is the band number, and $m = 1, 2$), and $\gamma_k = \arctan(|\rho(k)|/i\gamma)$, $\phi_k = \arg[\rho(k)]$. It clearly manifests the intrinsic Berry phase in the Hermitian case (i.e., $\Phi_0/2$) and the non-Hermitian-induced geometric phase. Note that the Berry phase in the Hermitian case $[\frac{\Phi_0}{2} = \oint_k idk\langle\psi_{0m}(k)|\partial/\partial k|\psi_{0m}(k)\rangle$, where ψ_{0m} is the eigenstate in the Hermitian system] equals zero when $c_1 > c_2$ and π when $c_1 < c_2$. The global Berry phase remains quantized independent of on site non-Hermitian modulation in our system (i.e., $\Phi_B^1 + \Phi_B^2 = \Phi_0$), revealing the same topological nature depending on the dimerization of the SSH model. Figures 1(d) and 1(f) show the real and imaginary parts of mode constants of two edge states [β_A and β_B], respectively, as the function of c_2/c_1 in a finite system ($N = 12$) with different gain or loss strength (γ). One can see that the split modes tend to merge to the exact-zero modes for the real part as γ increases, which finally reach the point of $c_2/c_1 = 1$ when $\gamma/c_1 = 0.24$. It indicates that those split near-zero modes are fully recovered by increasing the gain (loss) strength in such a non-Hermitian system with finite size. Correspondingly, the imaginary part splits, indicating the broken-PT symmetry.

In order to clearly demonstrate the recovery of zero modes, 2D diagrams of $|\mathrm{Re}(\beta_A - \beta_B)|$ and $|\mathrm{Im}(\beta_A - \beta_B)|$ are plotted as functions of the waveguide amount (N) and normalized gain or loss strength (γ/c_1) with $c_2/c_1 = 2$ in Figs. 2(a) and 2(b). A white guiding curve shows the boundary defined by exceptional points, as termed the EP boundary. As the N and γ/c_1 increase, crossing this EP boundary, we may find $|\mathrm{Re}(\beta_A - \beta_B)|$ gets to zero and $|\mathrm{Im}(\beta_A - \beta_B)|$ breaks to nonzero values. This implies that

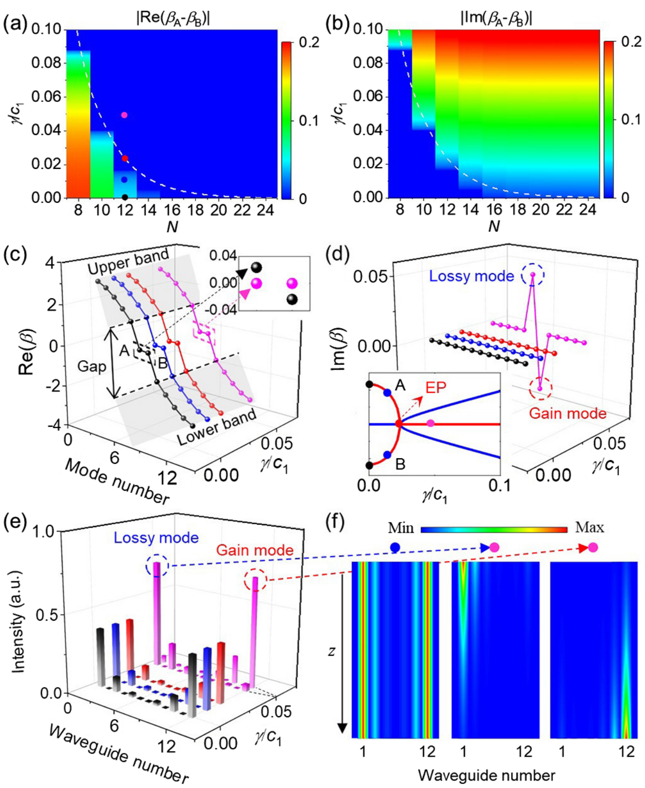

FIG. 2. Edge mode properties in the non-Hermitian SSH model. (a) $|\mathrm{Re}(\beta_A - \beta_B)|$ and (b) $|\mathrm{Im}(\beta_A - \beta_B)|$ as functions of N and γ/c_1 with $c_2/c_1 = 2$ (here $c_1 = 1$). The black, blue, red, and magenta dots mark the edge states shown in (c)–(e). (c) The real part of eigenvalues as functions of mode number and γ/c_1, where the gap modes A and B are particularly shown in the zoom-in inset figure. (d) The corresponding imaginary eigenvalue spectra, where the inset depicts the evolutions of real (red curves) and imaginary (blue curves) parts of modes A and B with respect to γ/c_1. (e) The mode profiles of the five edge states, in which two recovered zero modes (gain and lossy) are both presented. (f) CMT calculated field propagations of exact-PT-symmetric mode (the blue case with $\gamma/c_1 = 0.012$) and two zero modes in the broken-PT phase (the magenta case with $\gamma/c_1 = 0.05$).

one can recover the exact-zero modes either by increasing the system size (N) or the gain or loss strength (γ). Therefore, tuning γ is a good route to manipulate the zero modes in a defined finite system. For instance, we analyze the mode properties of TESs in the case of $N = 12$ with different γ values ($\gamma/c_1 = 0, 0.012, 0.023, 0.05$) marked as the black, blue, red, and magenta dots in Fig. 2(a). Two edge states in the Hermitian (black curve) and non-Hermitian cases with exact-PT symmetry (blue curve) have purely real mode constants that are slightly detuned from zero [see Fig. 2(c)], which corresponds to the localized optical intensities on both boundaries guaranteed by PT symmetry [see Fig. 2(e)]. As γ increases, the two edge states in their real energy spectra tend to be degenerated to an exact-zero state and their imaginary parts tend to split through the EP. This mode evolution is well displayed in the inset of Fig. 2(d), where the red and blue curves are for the real and imaginary parts (β_A, β_B), respectively. The recovered zero-energy states with a pure imaginary mode constant (magenta curves) localize on one side depending either on lossy or gain modes due to PT-symmetry breaking [see Fig. 2(e)]. Thus, the dissipative lossy mode finally sinks, and the other gain one rises [see the field propagations in Fig. 2(f)]. Detailed mode analyses on these TESs are provided in the Supplemental Material [40]. We further theoretically analyzed the robustness of the near- and exact-zero modes against structural fluctuations, which shows enhanced topological protection of recovered zero modes. It is further confirmed by our later experiments in a passive-PT system [40].

Afterwards, we carried out full-wave simulations (COMSOL MULTIPHYSICS 5.3) and experiments in a silicon waveguide platform based on passive-PT symmetry [3,7,29,42]. Here, we fix the total number of waveguides to $N = 12$, and the dissipative element consists of an array of lossy metal (i.e., chrome) stripes deposited on top of every other silicon waveguide, as shown in Fig. 3(a). The dynamic evolution of TESs in the optical lattice can be drastically altered by the synthetic dissipative PT-symmetric potential. The structural parameters such as waveguide width (w), height (h), and the gaps (g_1 and g_2) are optimized as $w = 400$, $h = 220$, $g_1 = 200$, and $g_2 = 120$ nm. Based on this design, only one fundamental mode is supported in the silicon waveguide at $\lambda = 1550$ nm with a propagation constant $\beta_0 = 2.1601\ k_0$ (k_0 is the free space k vector), and the waveguides have a coupling coefficient $c_1 = 0.0811$ and $c_2 = 0.1508\ \mu\mathrm{m}^{-1}$, respectively. The EP is derived at $2\gamma = 0.0053\ \mu\mathrm{m}^{-1}$, corresponding to 53-nm-wide and 4-nm-thick chrome (Cr) layer, where the loss is engineered by the width of the Cr strip (see Supplemental Material [40]). Figure 3(b) shows the evolution of the propagation constant of modes A and B with respect to loss 2γ. Here, we designed two lattices with 50- and 100-nm width (both in 4-nm thickness) Cr layers for the exact-PT and broken-PT phases, corresponding to $2\gamma = 0.005$ and $0.010\ \mu\mathrm{m}^{-1}$, respectively

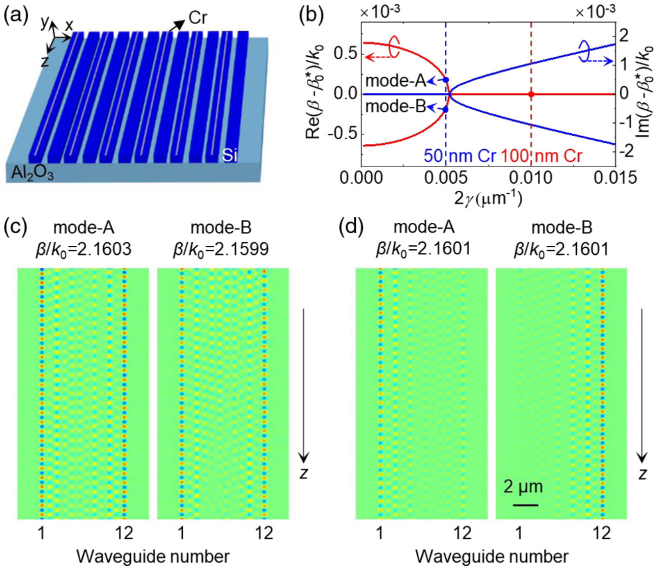

FIG. 3. Theoretical model and simulation results. (a) Schematic of the non-Hermitian optical lattice consisting of a dissipative *PT* silicon waveguide array, the additional chrome (Cr) layer on top of every other silicon waveguide to introduce periodic optical loss modulation. (b) Theoretical mode spectrum of the normalized mode constant as functions of the loss strength (2γ), where $\beta_0^* = \beta_0 + i\gamma$ is the averaged propagation constant in the passive system. Two particular cases of $2\gamma = 0.005\ \mu m^{-1}$ (exact-*PT* phase) and $2\gamma = 0.010\ \mu m^{-1}$ (broken-*PT* phase) are marked corresponding to the simulation and experimental parameters. Simulated field evolutions of the edge states in (c) exact-*PT* and (d) broken-*PT* phases with exactly prepared input excitation states.

[see blue and red dots in Fig. 3(b)]. It is clear that in the case of $2\gamma = 0.005\ \mu m^{-1}$ the normalized propagation constants of modes A and B are divergent from zero [$(\beta - \beta_0)/k_0 = \pm 0.0002$] resulting in $\beta_A/k_0 = 2.1603$ and $\beta_B/k_0 = 2.1599$ (here $\beta_0/k_0 = 2.1601$). Whereas they merge together to the exact-zero mode ($\beta_A = \beta_B = \beta_0$) as 2γ increases over the EP. To confirm this, the field propagations of both cases were simulated with the excitation states exactly retrieved from the theoretical calculations [Fig. 3(b)]. Figure 3(c) displays the field propagations of modes A and B in the exact-*PT* phase, which show a slight difference in phase symmetry and evolution corresponding to their different mode constants, and the unchanged two-boundary localizations in propagation definitely indicate their eigenmode property. As for the broken-*PT* case [see Fig. 3(d)], both modes show their one-sided field localizations with the same phase evolutions, indicating the same mode constant of the recovered exact-zero mode. Note that mode A is lossy with apparent decaying in intensity, while the other "gain" mode (mode B) does not.

The experimental samples were fabricated by *E*-beam lithography and an inductively coupled plasma etching process, followed by a second-step *E*-beam lithography with careful alignment and lift-off process to deposit the Cr stripes (see Supplemental Material [40]), which include the waveguide array, an input grating coupler, and extended output ports. The scanning electron microscopy (SEM) images of the fabricated structures are shown in Figs. 4(a)–4(c). It should be mentioned that there are two branch waveguides at the input ends, which were designed to prepare the eigenmodes of the TES [40]. In experiments, the light was input into the waveguide lattice by focusing the laser ($\lambda = 1550$ nm) via an input grating coupler. The transmitted signals can be collected from the scattered light from the extended output ports. The coupling-in and coupling-out processes were imaged by a near-infrared CCD camera (Xenics Xeva 1083). Figure 4(d) displays the optical propagations in experiments. The detailed output results of two kinds of samples captured by CCD are displayed in Figs. 4(e) and 4(f) (top panels). Moreover, we extracted the normalized intensity displayed in the bar diagrams [red bars, see the bottom panels in Figs. 4(e) and 4(f), respectively], which agree extremely well with the simulation results (blue bars). In the experiment of the exact-*PT* phase, the two-sided input only excites the near-symmetric mode of the two-sided edge states [i.e., mode B in Fig. 3(c)]. From Fig. 4(e), it is evident that this sample supports two-boundary TESs with *PT* symmetry,

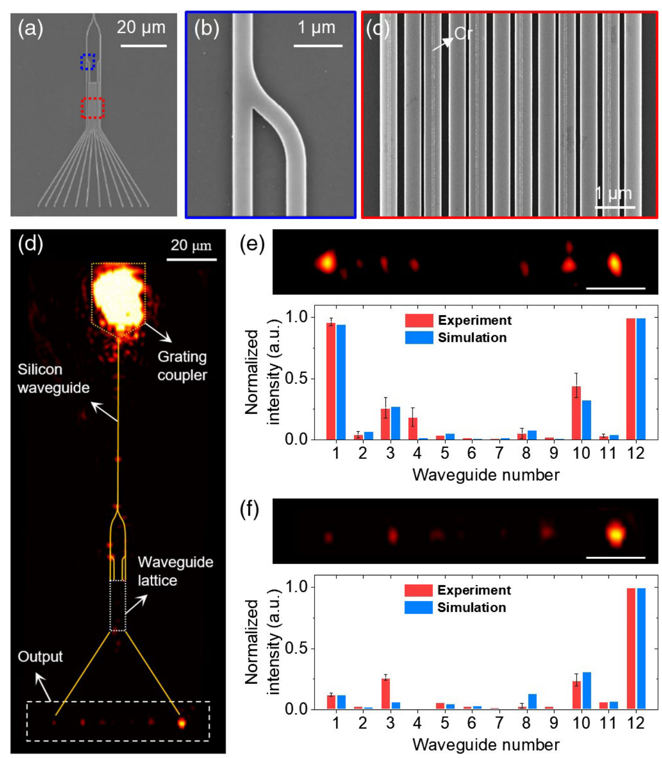

FIG. 4. Experimental results. (a)–(c) SEM image and enlarged regions of the fabricated structure. (d) CCD recorded optical propagation from input to output through the waveguide lattice. (e) Experimentally detected output intensities (top) and normalized intensity profiles (bottom) of near-zero mode B. (f) Corresponding results for the recovered exact-zero mode B (gain mode), where another lossy mode A decays off in propagation. Scale bar = 10 μm.

though the output intensities of the two boundaries are not exactly the same. This small deviation would mainly account for the imperfections of the eigenmode preparation and fabrications. As for the recovered exact-zero mode, it should be the one-sided eigenmode with degenerated mode constant. Here, our experiments still use two-sided excitation in order to get a direct comparison with the case of near-zero modes. Indeed, this two-sided excitation corresponds to two superposed eigenmodes, one is lossy (mode A) and the other is gain (mode B), as indicated in Fig. 3(d). Because of the decaying mode A, we eventually observed the gain mode B in experiments [Fig. 4(f)], confirming the recovered zero mode in broken-PT symmetry. These experimental and simulation results are in good agreement, which well prove our theoretical predictions. According to more experimental results, we find that the exact-PT-symmetric modes are more sensitive to the structural perturbations because they are not exact-zero modes, while the recovered zero modes exhibit more robustness (see Supplemental Material [40]).

Now, we have confirmed that in a finite topological system, the zero modes of edge states will break due to the coupling between them. More interestingly, these modes can be further recovered by non-Hermitian degeneracies through loss modulation. This recovery can be intuitively explained in that these gain or loss modulations in the waveguide lattice can indeed reduce the coupling of the boundary modes. In addition, we further demonstrated the different field evolutions of the near-zero and exact-zero modes with single-side excitation [40]. It turns out that the former exhibits a boundary coupling phenomena (i.e., field energy transfer between the two boundaries), while the latter (the exact-zero mode) keeps good localization along the preferred boundary.

In conclusion, we have exploited the breakup and recovery of photonic zero modes in the SSH model by tuning the loss to form a non-Hermitian configuration. The experimental results on finite silicon waveguides with controlled loss are fully consistent with the theoretical prediction. Since many realistic topological systems have finite size, their topological edge states should not be the exact ones and will be degraded by structural imperfections. The recovered zero modes by introducing the non-Hermitian item exhibit enhanced topological protection compared with the Hermitian cases. Our results show that the topological property can be manipulated by non-Hermitian parameters, which should inspire more insightful explorations in topological and PT photonics.

The authors acknowledge the financial support from The National Key Research and Development Program of China (2017YFA0303701, 2016YFA0202103), National Natural Science Foundation of China (Grants No. 91850204, No. 11674167, No. 11621091). T. L. is thankful for the support from Dengfeng Project B of Nanjing University.

[*]Corresponding author.
taoli@nju.edu.cn

[1] C. M. Bender and S. Boettcher, Phys. Rev. Lett. **80**, 5243 (1998).
[2] S. Klaiman, U. Günther, and N. Moiseyev, Phys. Rev. Lett. **101**, 080402 (2008).
[3] A. Guo, G. J. Salamo, D. Duchesne, R. Morandotti, M. Volatier-Ravat, V. Aimez, G. A. Siviloglou, and D. N. Christodoulides, Phys. Rev. Lett. **103**, 093902 (2009).
[4] R. El-Ganainy, K. G. Makris, D. N. Christodoulides, and Z. H. Musslimani, Opt. Lett. **32**, 2632 (2007).
[5] C. E. Rüter, K. G. Makris, R. El-Ganainy, D. N. Christodoulides, M. Segev, and D. Kip, Nat. Phys. **6**, 192 (2010).
[6] A. Regensburger, C. Bersch, M. A. Miri, G. Onishchukov, D. N. Christodoulides, and U. Peschel, Nature (London) **488**, 167 (2012).
[7] L. Feng, Y.-L. Xu, W. S. Fegadolli, M.-H. Lu, J. E. B. Oliveira, V. R. Almeida, Y.-F. Chen, and A. Scherer, Nat. Mater. **12**, 108 (2013).
[8] L. Chang, X. Jiang, S. Hua, C. Yang, J. Wen, L. Jiang, G. Li, G. Wang, and M. Xiao, Nat. Photonics **8**, 524 (2014).
[9] B. Peng, S. K. Özdemir, F. Lei, F. Monifi, M. Gianfreda, G. L. Long, S. Fan, F. Nori, C. M. Bender, and L. Yang, Nat. Phys. **10**, 394 (2014).
[10] L. Feng, Z. J. Wong, R.-M. Ma, Y. Wang, and X. Zhang, Science **346**, 972 (2014).
[11] H. Hodaei, A. U. Hassan, S. Wittek, H. Garcia-Gracia, R. El-Ganainy, and, D. N. Christodoulides, Nature (London) **548**, 187 (2017).
[12] W. Chen, S. K. Özdemir, G. Zhao, J. Wiersig, and L. Yang, Nature (London) **548**, 192 (2017).
[13] L. Lu, J. D. Joannopoulos, and M. Soljačić, Nat. Photonics **8**, 821 (2014).
[14] T. Ozawa, H. M. Price, A. Amo, N. Goldman, M. Hafezi, L. Lu, M. C. Rechtsman, D. Schuster, J. Simon, O. Zilberberg, and I. Carusotto, Rev. Mod. Phys. **91**, 015006 (2019).
[15] *Topological Insulators*, edited by M. Franz and L. Molenkamp, Contemporary Concepts of Condensed Matter Science Vol. 6 (Elsevier, Amsterdam, 2013).
[16] S. Ryu and Y. Hatsugai, Phys. Rev. Lett. **89**, 077002 (2002).
[17] A. Blanco-Redondo, I. Andonegui, M. J. Collins, G. Harari, Y. Lumer, M. C. Rechtsman, B. J. Eggleton, and M. Segev, Phys. Rev. Lett. **116**, 163901 (2016).
[18] Q. Cheng, Y. Pan, Q. Wang, T. Li, and S. Zhu, Laser Photonics Rev. **9**, 392 (2015).
[19] S. D. Liang and G. Y. Huang, Phys. Rev. A **87**, 012118 (2013).
[20] J. M. Zeuner, M. C. Rechtsman, Y. Plotnik, Y. Lumer, S. Nolte, M. S. Rudner, M. Segev, and A. Szameit, Phys. Rev. Lett. **115**, 040402 (2015).
[21] L. Ge, Phys. Rev. A **95**, 023812 (2017).
[22] S. Lieu, Phys. Rev. B **97**, 045106 (2018).
[23] B. Midya, H. Zhao, and L. Feng, Nat. Commun. **9**, 2674 (2018).
[24] W. Zhu, X. Fang, D. Li, Y. Sun, Y. Li, Y. Jing, and H. Chen, Phys. Rev. Lett. **121**, 124501 (2018).
[25] L. Xiao, X. Zhan, Z. H. Bian, K. K. Wang, X. Zhang, X. P. Wang, J. Li, K. Mochizuki, D. Kim, N. Kawakami, W. Yi,

H. Obuse, B. C. Sanders, and P. Xue, Nat. Phys. **13**, 1117 (2017).
[26] S. Weimann, M. Kremer, Y. Plotnik, Y. Lumer, S. Nolte, K. G. Makris, M. Segev, M. C. Rechtsman, and A. Szameit, Nat. Mater. **16**, 433 (2017).
[27] C. Poli, M. Bellec, U. Kuhl, F. Mortessagne, and H. Schomerus, Nat. Commun. **6**, 6710 (2015).
[28] K. Takata and M. Notomi, Phys. Rev. Lett. **121**, 213902 (2018).
[29] M. Pan, H. Zhao, P. Miao, S. Longhi, and L. Feng, Nat. Commun. **9**, 1308 (2018).
[30] G. Harari, M. A. Bandres, Y. Lumer, M. C. Rechtsman, Y. D. Chong, M. Khajavikhan, D. N. Christodoulides, and M. Segev, Science **359**, eaar4003 (2018).
[31] M. A. Bandres, S. Wittek, G. Harari, M. Parto, J. Ren, M. Segev, D. N. Christodoulides, and M. Khajavikhan, Science **359**, eaar4005 (2018).
[32] H. Zhao, P. Miao, M. H. Teimourpour, S. Malzard, R. El-Ganainy, H. Schomerus, and L. Feng, Nat. Commun. **9**, 981 (2018).
[33] M. Parto, S. Wittek, H. Hodaei, G. Harari, M. A. Bandres, J. Ren, M. C. Rechtsman, M. Segev, D. N. Christodoulides, and M. Khajavikhan, Phys. Rev. Lett. **120**, 113901 (2018).
[34] W. P. Su, J. R. Schrieffer, and A. J. Heeger, Phys. Rev. Lett. **42**, 1698 (1979).
[35] P. St-Jean, V. Goblot, E. Galopin, A. Lemaître, T. Ozawa, L. L. Gratiet, I. Sagnes, J. Bloch, and A. Amo, Nat. Photonics **11**, 651 (2017).
[36] J. Zak, Phys. Rev. Lett. **62**, 2747 (1989).
[37] P. Delplace, D. Ullmo, and G. Montambaux, Phys. Rev. B **84**, 195452 (2011).
[38] A. N. Poddubny, A. E. Miroshnichenko, A. P. Slobozhanyuk, and Y. Kivshar, ACS Photonics **1**, 101 (2014).
[39] A. P. Slobozhanyuk, A. N. Poddubny, A. E. Miroshnichenko, P. A. Belov, and Y. S. Kivshar, Phys. Rev. Lett. **114**, 123901 (2015).
[40] See Supplemental Material at http://link.aps.org/supplemental/10.1103/PhysRevLett.123.165701 for (i) the field distributions of edge states in the SSH model, (ii) a comparison of robustness of near-zero and exact-zero modes, (iii) the experimental characterization of loss and coupling coefficients, (iv) sample fabrication details, (v) the input state control of TESs, and (vi) the field evolutions of the near-zero and exact-zero modes with single-side excitation, which includes Refs. [3,26,41].
[41] A. D. Rakic, A. B. Djurisic, J. M. Elazar, and M. L. Majewski, Appl. Opt. **37**, 5271 (1998).
[42] Y.-L. Xu, W. S. Fegadolli, L. Gan, M.-H. Lu, X.-P. Liu, Z.-Y. Li, A. Scherer, and Y.-F. Chen, Nat. Commun. **7**, 11319 (2016).